

Effect of SST Variation on ITCZ in APE Simulations

K. RAJENDRAN

C-MMACS, National Aerospace Laboratories, Bangalore, India

A. KITO^H*

Meteorological Research Institute, Tsukuba, Japan

J. SRINIVASAN

Indian Institute of Science, Bangalore, India

(Journal of Met. Soc. Japan, Revised on 10 Jun 2010)

Corresponding author address:

Dr. Akio Kitoh,

Climate Research Department, Meteorological Research Institute (MRI),

1-1 Nagamine, Tsukuba, Japan. 305 0052

E-mail: kitoh@mri-jma.go.jp

Abstract

The effect of meridional variation of sea surface temperature (SST) on tropical atmospheric circulation is analyzed using Aqua-planet Experiment (APE) simulations. The meridional SST gradient around the narrow SST peak in *Control* simulation favours a strong and single equatorial Inter Tropical Convergence Zone (ITCZ, defined by the maximum of zonally averaged total precipitation) in all APE models. In contrast, flat equatorial SST peak (*FLAT* simulation) favours split/double ITCZs flanking the SST maximum, in the majority of the APE models. Although there is reasonable agreement for SST sensitivity of ITCZ among the APE models in *Control*, there exists disparity among them in *FLAT* case. Similarly, while the total and convective precipitation responses are consistent among the models, the large-scale precipitation response shows considerable inter-model variations in *FLAT* case. The APE intercomparison indicates that the occurrence and positioning of the ITCZ are primarily related to boundary layer moisture convergence as a response to the meridional variation of SST. Furthermore, the meridional gradient of tropospheric temperature is found to be an important factor that can influence the positioning of ITCZ.

FLAT SST distribution is found to be similar to the observed distribution over the Indian region during summer season. Models that yield double ITCZs in this case simulate an easterly jet over the equatorial region ($\sim 15^\circ$ equatorward of the ITCZ). This is analogous to the Tropical Easterly Jet (TEJ), which is a unique feature observed over the Indian region during summer monsoon season, with its core at 12°N , equatorward of the seasonal convergence zone centered along 25°N . In these models, positive meridional temperature gradient and the associated easterly shear in the atmosphere strengthened by

moisture convergence penetrate up to the upper troposphere, with which TEJ is in thermal wind balance.

1. Introduction

There have been numerous observational, theoretical and numerical modeling studies on the physical mechanisms regulating the formation and latitudinal preference of the Inter-tropical Convergence Zone (ITCZ). The earliest attempts tried to relate the spatial distributions of sea surface temperature (SST) to the spatial structure of tropical convection. These were motivated by the observed high correlation between convective enhancement and warm SST forcing as found by Bjerknes (1969). This was also supported by a number of numerical simulations (Pike 1971; Manabe et al. 1974). Lindzen and Nigam (1987) suggested that dynamically induced low-level convergence resulting from SST gradients can be usefully viewed as a cause of deep convection on climatological scales. Recently, a study by Back and Bretherton (2009) using a linear mixed layer model showed that surface convergence patterns on long time scales are strongly related to SST gradient.

Aquaplanets have been used in several contexts in atmospheric modeling studies. This approach includes the full complexity of atmospheric general circulation model (AGCM) parameterizations, but simplifies the lower-boundary condition by defining a less complex surface with symmetries in its specification and in the external forcing. Many studies using aquaplanet GCMs addressed the relationship between SST and the location and intensity of the ITCZ. But it was found that SST forcing alone cannot explain all observed features, and considerable variation was found to exist in the relationship of convection to the underlying SST distribution. For example, observational studies showed that the highest SST is often not collocated with the ITCZ (Ramage 1974; Sadler 1975; Hastenrath and Lamb 1977; Lietzke et al. 2001). Modeling studies (Hayashi

and Sumi 1986; Hess et al. 1993; Waliser and Somerville 1994) also showed that double ITCZs develop straddling the equator even if the SST maximum is at the equator. Also it was found that a well-defined ITCZ can still occur in numerical simulations with globally uniform SST (Sumi 1992; Chao 2000) implying that inhomogeneous SST forcing might not be necessary. These studies indicate that the dynamical processes likely play an important role in regulating the ITCZ.

The position and intensity of ITCZ were often found to depend on the location of the maximum SST and the type of deep convection parameterization used in the GCM. Hayashi and Sumi (1986) using a zonally symmetric SST with maximum located at the equator in a GCM with Kuo convection scheme found that double ITCZs exist on 7°N and 7°S. The intensity of the Hadley circulation were made to appear similar to the observed circulation by shifting the location of the heat source (Lindzen and Hou 1988). Simulated ITCZ structure was also found to be associated with the implemented convective parameterization. A single precipitation maximum developed at the latitude of maximum SST with the moist convective adjustment scheme in the GFDL model (Lau et al. 1988), the JMA model (Numaguti and Hayashi 1991a) and the NCAR model (Hess et al. 1993), and with the Arakawa-Schubert scheme in the MRI GCM (Ose et al. 1989). Meanwhile, double ITCZ structure straddling the SST maximum developed with the Kuo convective parameterization in the JMA model (Hayashi and Sumi 1986; Numaguti and Hayashi 1991a) and NCAR model (Hess et al. 1993) and with the Lyne and Rowntree convection parameterization scheme in the UKMO model (Swinbank et al. 1988). On the other hand, a mass flux scheme with the Kuo-type moisture convergence closure was found to simulate a single ITCZ (Lorant and Royer 2001) that develops into slightly split

ITCZs when a more sophisticated vertical diffusion scheme is coupled to a statistical cloud scheme. Similarly, Hess et al. (1993) also found that the Kuo scheme tends to simulate a single peak if the warmest water is flanked by very strong meridional SST gradients. Numaguti and Hayashi (1991b) and Numaguti (1993) also found that with increased latent heat flux in the equatorial region, the Kuo scheme resulted in a single ITCZ rather than the double structure in the *Control* version.

It is important to verify these findings in current state of the art General Circulation Models (GCMs) to understand the factors controlling the position and intensity of the ITCZ. Recently, Neale and Hoskins (2000a) proposed Aqua Planet Experiments (APE) comprising a suite of aquaplanet simulations as a standard test for AGCMs including their physical parameterizations. A large spectrum of the state-of-the-art atmospheric GCMs in aqua-planet configuration were forced with a standard set of SST forcings. In this study, we analyze and intercompare the APE simulations, in order to study the effect of SST variation on ITCZ and to understand the dynamical processes that regulate the latitudinal preference of equatorial ITCZ. In addition, we discuss the implication of the APE intercomparison for tropical circulation. Section 2 introduces the APE models and the details of the SST distributions prescribed for the three types of APE simulations. Section 3 explores the role of meridional gradient of SST in the precipitation response of the participating models. Section 4 extends the ideas of the previous section, connecting the dynamic and thermodynamic effects on changes in precipitation response among the APE models. Following that, Section 5 discusses the tropical circulation response in the APE models to different SST forcings and its implication for tropical easterly jet associated with the Indian summer monsoon. Section 6 provides a brief

summary.

2. APE Simulations

The aquaplanets that join the APE project are forced by a family of prescribed SST distributions, which vary only with latitude in the absence of any sea ice. In these experiments, perpetual equinoctial orbital parameters remove seasonal variations in insolation, but the diurnal variability is preserved. Despite the simplified boundary condition, the full GCM dynamics and physics are retained. In this study, we analyze simulations of 13 participating models of the APE project. The details of these models and modeling groups are given in Table 1. They differ with respect to various features such as resolution, physics, dynamics and numerics.

a. SST Boundary Forcings

Under the APE project, five cases are defined with zonally symmetric SSTs to study the response to different SST gradients, and three cases with zonally asymmetric SSTs (Neale and Hoskins 2000b). In the zonally symmetric cases, the specified SST gradient varies from almost flat in the deep tropics to a strong gradient all the way to the equator. We analyze APE simulations that were forced with three of these zonally symmetric SSTs, viz. *Control*, *Q_{obs}*, and *FLAT*. The selected case of *Q_{obs}* represents an intermediate distribution of SST between those of *Control* and *FLAT*. SST profiles for these three axisymmetric cases are explained in Table 2. The corresponding latitudinal variation of SST, and meridional gradient and second derivative of SST are shown in Fig. 1. All the three profiles are symmetric about the equator. In *Control* distribution, there is stronger meridional SST gradient flanking the equator, *Q_{obs}* has a wider SST maximum around the equator and *FLAT* has the widest SST maximum with widest zero gradient of SST around the equator.

b. Experimental Strategy

Each APE experiment is started from a model-simulated state, obtained from either an earth-like simulation or a previous aqua-planet integration. The simulation period is 3.5 years for each experiment and the first half year is excluded from analysis as a spin up period, after confirming that equilibration was achieved during this period. The mean state of all the variables used in this study, is the average over the 3-year simulation period.

c. Observed Datasets

Observed and analyzed datasets of precipitation and circulation are used to analyze important features of tropical circulation. We have used monthly GPCP precipitation data on $2.5^\circ \times 2.5^\circ$ grid for the period 1979-2002 (Adler et al. 2003). Circulation fields for the period 1979-2002 from ERA-40 reanalysis (Uppala et al. 2005) are also used. The primary reference and a full report documenting the data set for the reanalysis can be found at <http://www.ecmwf.int/research/era/>. We have also used the Hadley Centre, United Kingdom monthly SST (HadISST) data (Rayner et al. 2003) on a $2.5^\circ \times 2.5^\circ$ grid for 1979-2002 period.

3. Meridional SST gradient and ITCZ

Figure 1 shows the latitudinal variation of SST (dashed line), and the meridional gradient (solid line) and the second derivative (dotted line) of SST for *Control*, *Qobs* and *FLAT* simulations. In *Control* simulation, SST maximum is located just over the equator with sharp reduction on either side of the equator. Correspondingly, meridional gradient of SST is zero at the equator where its derivative is minimum. SST gradient gradually increases towards higher latitudes and maximizes at 30° away from the equator. In *FLAT* simulation, the SST maximum and the zero SST gradient at the equator are much broader

than those in *Control* simulation, and meridional SST gradient maxima flanking the equator are shifted by 7.5° farther from their corresponding positions in *Control* simulation. Corresponding latitudinal variations of SST and its first and second derivatives for *Qobs* show that it is an intermediate case between *Control* and *FLAT* simulations.

Figure 2 shows how the specification of the underlying SST affects the total precipitation in *Control*, *Qobs*, and *FLAT* simulations. In this analysis, ITCZ in a particular APE simulation is defined as the maximum of zonally averaged total precipitation. The *Control* distribution favours a single or narrow ITCZ over the equator in the APE models. As the peak of the equatorial SST flattens, the single precipitation peak is gradually replaced by two precipitation peaks flanking the equator in many models (*e.g.*, *Qobs* simulation). This indicates that spatial organization and dynamics of convective structures strongly depend on latitudinal distribution of SST. As the meridional gradient of SST starts changing around the narrow SST maximum at the equator in *Control* (Fig. 1), a strong and single or narrow equatorial ITCZ develops between 5°N - 5°S in all the models except for a minor tendency for a relative minimum at the equator in few models. In contrast, flatter equatorial SST maximum (in *Qobs* and *FLAT*) favours split ITCZs occurring at SST gradients between $0.2^\circ\text{C}/\text{deg}$ and $0.3^\circ\text{C}/\text{deg}$, flanking the SST maximum in many models. The broad equatorial SST maximum in *FLAT* simulation results in distinct double ITCZs with peaks located between 12° and 17° on both sides of the equator, in the majority of the APE models. Thus, the precipitation response clearly indicates that broadening of SST maximum gives rise to split ITCZs. Although there is reasonable agreement for the SST sensitivity of ITCZ among the APE models in the *Control* case, there exists strong disparity as the equatorial SST maximum flattens. For example, in *FLAT* case, some of the models simulate either predominantly equatorial ITCZ or split ITCZs with peaks within the equatorial region of 5°N - 5°S

(LASG, AGU, K1-JAPAN and MIT). The precipitation response in Q_{obs} appears to have hybrid characteristics between those in *Control* and *FLAT* simulations. Hence, further results are presented only for *Control* and *FLAT* SST simulations. The distribution of precipitation minus evaporation ($P-E$) is a useful quantity for understanding the ITCZ position, where mean precipitation exceeds evaporation. Figure 3 shows the latitudinal variation of zonally averaged $P-E$ in *Control* and *FLAT* simulations. It can be seen that the maximum of $P-E$ coincides with the ITCZ in both cases.

To understand the reasons for the disparity among APE models in simulating the precipitation response to *FLAT* SST distribution, we have selected models with extreme SST sensitivity based on two criteria; (i) $P-E > 0$ over the equator, and (ii) total precipitation $> 4\text{mm/day}$ at the equator. There are four models (AGU, K1-JAPAN, LASG and MIT) satisfying the two conditions which either simulate single equatorial ITCZ or split ITCZ over the near-equatorial latitudes. These models differ considerably in simulating the ITCZ response to latitudinal variation of SST when compared to majority of the models in *FLAT* case. While LASG has strong tendency to simulate single ITCZ for any of the equatorially symmetric SST forcings, K1-JAPAN and MIT still simulate precipitation peaks near the equator, with *FLAT* SST forcing. Thus, to further study the two different types of precipitation response to *FLAT* SST forcing, the APE simulations are grouped into two categories; models with distinct double ITCZs form the first category and the rest of the models satisfying the above two criteria (AGU, K1-JAPAN, LASG and MIT) form the second category. It is difficult to derive the influence of convection parameterization alone for these two categories of simulations. Nevertheless, two models whose convection schemes lack explicit trigger for convection (AGU with the Emanuel scheme and LASG with the MCA scheme) are found to give rise to a single ITCZ, as reported by previous studies (Lau et al. 1988; Numaguti and Hayashi 1991a; Hess et al. 1993). Some of the first category of models, which show a strong tendency for

split ITCZs, use sophisticated convection schemes (CGAM and UKMO with the Gregory and Rowntree convection scheme; NCAR with the Zhang and McFarlane deep convection scheme).

Next, the relative contributions of convective and large-scale precipitation to total precipitation response in APE simulations are analyzed. The latitudinal variation of zonally averaged convective precipitation and large-scale precipitation simulated with the *Control* and *FLAT* SST profiles are shown in Fig. 4 and Fig. 5 respectively. Convective precipitation variation closely follows that of total precipitation for both cases. However, there are large differences between convective and large-scale precipitation amounts. It is important to note that, while the total and convective precipitation responses are more or less consistent among the APE models (Fig. 2 and Fig. 4), the large-scale precipitation response (Fig. 5) shows considerable variations among the models for the *FLAT* SST case. This may be due to differences in dynamics among the APE models.

4. Role of boundary layer moisture convergence

Precipitation response to the prescribed SST forcing can be interpreted based on budgets of moisture and dry static energy for the ITCZ (Srinivasan 2001, 2003). Srinivasan (2003) combined the energy and moisture balance equations into a simplified form suited for the tropics and suggested that one of the important parameters that determine the location and strength of the ITCZ is the stability factor primarily determined by the column integrated water vapor (P_w). Hence, factors that affect the net energy convergence and column water vapor are important in determining the structure of $P-E$. Accordingly, in the APE simulations, it is seen that the vertically integrated specific humidity shows distinct behaviour against $P-E$ in response to latitudinal variation of SST. Figure 6 compares latitudinal variation of $P-E$ with vertically integrated specific humidity q for *Control*, and *FLAT* simulations of three representative models from the

two categories. The first category of those models with double ITCZs in *FLAT* case are shown in the right panels, and second category of models are shown in the left panels. The latitudinal variation of fq closely follows $P-E$ in *Control* and *FLAT* cases. In the first category of models, the latitudinal variation of fq also shows a tendency to yield double peaks in the variation of $P-E$ in the *FLAT* case. In contrast, in the second category of models, latitudinal variation of fq shows a broad peak around the equator that follows $P-E$ variation with *FLAT* SST forcing.

Zonally and vertically averaged moisture conservation on the monthly mean scale can also be written as:

$$P - E \propto - \int \left[\frac{\partial(qV)}{\partial y} \right] \frac{dp}{g} = - \left[\int q \frac{\partial(V)}{\partial y} + \int V \frac{\partial(q)}{\partial y} \right] \frac{dp}{g} \quad (1)$$

where P denotes precipitation, E evaporation, q specific humidity, V meridional velocity, g acceleration due to gravity and p pressure. In this case, the contributions from zonally asymmetric eddies are considered to be negligible. Thus, vertically integrated meridional convergence is proportional to mass convergence and moisture advection into the column.

Our analysis of the vertical profile of the zonally averaged quantities of these two terms showed that the moisture convergence corresponds well with the latitudinal variation of ITCZ, in majority of APE simulations. For example, Fig. 7 shows the latitude-height section of zonally averaged moisture convergence in MRI model for two SST profiles of *Control* and *FLAT*. In *Control*, moisture convergence maximizes at the equator, whereas in *FLAT*, there are two distinct convergence maxima flanking the equator corresponding to the double ITCZs. Here, the convergence extends homogeneously up into the mid-troposphere. Outside the ITCZ region, there are moisture divergence in the boundary layer. Thus, for the majority of models that produced the double ITCZ with flattened SST, the $P-E$ could be interpreted in terms of the impact of SST gradients on the meridional mass convergence of moist air in the boundary layer.

Since specific humidity decreases rapidly with height, vertically integrated meridional moisture convergence is dominated by meridional mass convergence in the boundary layer. The latitudinal variation of $P-E$ against low-level mass convergence of moist air for three representative models of each of the two categories are shown in Fig. 8. The boundary layer mass convergence peaks are collocated with the ITCZs in all the models. However, in *FLAT* simulations of the first category of models, the latitudinal variation of low-level mass convergence shows a double peak structure consistently with that of $P-E$. The response in the majority of the simulations to the two SST forcings clearly suggests that the an impact of meridional gradient of SST on boundary layer mass convergence of moist air is a decisive factor for the positioning of ITCZs. This is consistent with the findings of theoretical studies such as Lindzen and Nigam (1987) and Back and Bretherton (2009), which suggested that boundary layer convergence is primarily a function of the pattern of SST gradients and is better regarded as a cause rather than a consequence of deep convection.

5. Zonally Symmetric Circulation Response

Latitudinal distributions of difference in temperature relative to equatorial temperature at the 850 hPa and 200 hPa levels for *Control* and *FLAT* cases are shown in Fig. 9. At 850 hPa, influence of underlying SST is very strong in all the models where the latitudinal distributions of temperature difference for both cases are similar to that of the respective SST. The region with weak gradient seems to be the preferred region for ITCZ formation, as seen in Fig. 1 and Fig. 2. In *FLAT* SST case, this region widens on either side of the equator. In contrast, the corresponding distribution at 200 hPa is much flatter and different from that of underlying SST. In the majority of the models, there is a tendency of reduction in meridional temperature gradient or even its sign reversal at the equatorial latitudes. This region widens as the underlying SST maximum flattens. The upper-level

heating associated with the off-equatorial ITCZs can be due to condensational heating of moisture. Here it should be noted that an earlier study on the African easterly Jet (Thorncroft and Blackburn 1999) has suggested the possibility of the jet being located at the level of such temperature gradient reversal over the ITCZ.

Figure 10 shows latitude-height cross sections of meridional variation of temperature $\left(\frac{\partial T}{\partial y}\right)$ for two representative models of the two categories of simulations, for *Control* and *FLAT* SST forcings. It can be seen that in a model that does not yield double ITCZs for the flattened equatorial SST maximum (with zero SST gradient, *e.g.*, AGU), there is no marked change in the vertical profile of meridional temperature gradient between *Control* and *FLAT* simulations. In contrast, in a model that yields double ITCZs under the *FLAT* SST forcing, the meridional temperature gradient has the same sign in both the upper (500 hPa – 200 hPa) and lower (below 500 hPa) troposphere, in the deep tropics (10°S-10°N), which differs completely from *Control* case.

a. Implications: Tropical Easterly Jet

Figure 11 shows the meridional sections of zonally averaged zonal wind velocity and meridional circulation (v,w) for the simulations by three representative models of the first category, *i.e.*, MRI, ECMWF and NCAR models with *Control* and *FLAT* SST forcings. In *Control* case, there is low-level meridional convergence and ascent associated with an equatorial ITCZ. At upper levels, strong westerly jets are located on either a deep side of the ITCZ region. In *FLAT* case, strong low-level convergence and ascending are located away from the equator collocating with ITCZs (Fig. 2). The striking feature in this case, is the appearance of a distinct upper level easterly jet around 200 hPa over the equatorial region. This is associated with subsidence, which is particularly strong in the MRI and NCAR models. The equatorial easterly jet is under the thermal wind balance. The jet is accompanied by particularly strong temperature gradients that are consistent throughout

the mid and lower troposphere (as in Fig. 10), which appears to be an important factor for the jet formation in addition to the SST distribution. The heat flux from the surface can be transported upward and then in the middle and upper troposphere by deep cumulus convection.

Simulation of this equatorial easterly jet stream with *FLAT* SST forcing has important implications for Indian summer monsoon. Latitudinal distribution of observed climatological SST from HadISST averaged over warm tropical oceans are shown in Fig. 12. It can be seen that meridional distribution of SST in the *FLAT* case resembles that observed in the Bay of Bengal (BoB) during the summer monsoon season, though displaced by $\sim 10^\circ$ northward. Over the tropical oceans, only monsoonal warm pools of the BoB and western Pacific (WPac) have meridional SST variations similar to the *FLAT* distribution. Figure 13a shows the observed climatologies (1980-2000) of July precipitation (GPCP) and zonal wind velocity (ERA-40) at 150 hPa over the tropics. Over the longitudinal sector including the Bay of Bengal (70° - 90° E), the flattened seasonal SST maximum centered around 10° N (Fig. 12) is associated with double ITCZ structure where the northern branch corresponds to a continental ITCZ located around $\sim 25^\circ$ N and the southern branch to a maritime ITCZ located over the equatorial south Indian Ocean. This is a unique feature observed only over this longitudinal sector. Associated with this, there is an upper level zonal wind maximum in the form of a strong easterly jet with its core at 12° N, *i.e.*, about 13° southward of the primary continental rainbelt along the seasonal monsoon trough over India and 13° north of the maritime ITCZ. This is a strong monsoon component and a prominent large-scale monsoon circulation feature called the tropical easterly jet (TEJ), which is observed only over the Indian longitudes during the summer monsoon season (Koteswaram 1958). A meridional section of zonal wind velocity at 70° E based on ERA-40 is shown in Fig. 13b. The easterly jet core located

between the 100 and 150 hPa levels is well-defined with core velocity that is twice as strong as that of the monsoon westerlies at the surface. TEJ is an important component in the monsoon circulation, in addition to the subtropical westerly jet (SWJ) and cross equatorial surface westerly flow. As observed during the monsoon season, for the *FLAT* SST profile, an easterly jet is simulated over the equator between the dual ITCZs in some models of the first category as shown in Fig. 11. Thus, factors responsible for the TEJ formation are found to include the strong latitudinal temperature gradient throughout the equatorial troposphere, associated with double ITCZ structure that forms over the meridionally broad warm ocean.

b. Geostrophic Balance

To further understand the formation of the TEJ in the APE simulations, we investigate the degree to which the jet is geostrophic. In geostrophic motion, the horizontal component of the Coriolis force and pressure gradient force are in balance.

$$Ug = -\frac{1}{f} \left(\frac{\partial \phi}{\partial y} \right) \quad (2)$$

where Ug is the zonal component of geostrophic wind and f is the geopotential height. Meridional section of zonal wind velocity (U) for the MRI model for *Control* and *FLAT* cases and the corresponding zonal component of geostrophic wind (Ug) are shown in Fig. 14. It can be clearly seen that vertical distribution of U and Ug agree well between the two cases, indicating that the zonal wind is mostly geostrophic. The formation of the upper-level easterly jet in this model in *FLAT* case is evident in both components. The jet core is simulated around 200 hPa, slightly below the observed position between 150 hPa and 100 hPa. The jet forms in the same manner as in other models of the first category in *FLAT* case. In contrast, in the second category of models with predominant equatorial ITCZ in *FLAT* case, no easterly jet forms at the equator. This may be due to their unique nature of interaction between deep convection and dynamics in those models.

Since the easterly jet is essentially geostrophic, the easterly shear is associated with positive meridional temperature gradient below the level of the jet maximum (*e.g.*, Burpee 1972). Then, understanding of the easterly jet is equivalent with understanding the surface meridional temperature gradient and its communication into the free atmosphere. In order for the jet to form, the low-level temperature gradient must be positive and strong enough for the associated wind shear to form an easterly flow. Then the jet maximum corresponds to the pressure level where positive temperature gradient turns into negative gradient (Fig. 11) in the free atmosphere (Burpee 1972), or as argued by Thorncroft and Blackburn (1999), where the vertical temperature profile follows the dry adiabat and then the moist adiabat. Thus, if the nature of the diabatic forcing differs among models, for example, arising from different parameterization of deep cumulus convection or dry convection, then the simulated TEJ is likely to be different from one model to another in spite of the same boundary SST forcing.

Factors hypothesized to be important for tropical climate simulations include model resolution, and physics. Among the APE models with the same horizontal resolution, some of them do simulate clear double ITCZs with flattened SST (*e.g.*, MRI and NCAR), while some others yield a single equatorial ITCZ (*e.g.*, K1-JAPAN). Therefore, consistent resolution dependence of the SST sensitivity is not seen among the APE models. The 13 models analyzed in this study exhibit a large variety of model physics, including the major deep convection schemes with different types of convective closures, convective triggers, and cloud models (Table 1). Among the models with the same deep convection scheme (*i.e.*, MIT, GFDL and GSFC), the GFDL and GSFC models fall in the first category while MIT in the second category. Similarly, K1-JAPAN and MRI use the same convection scheme and horizontal resolution but fall in different categories of SST sensitivity. At the same time, many models have convection schemes that are similar to the Arakawa and Schubert (1974) scheme, but sometimes with a bulk cloud model instead of a spectral cloud model. However, among these models, there is a

hint that models with explicit moisture trigger tend to simulate double ITCZs with *FLAT* SST (*e.g.*, NCAR, CGAM and UKMO). Also, the LASG model with Moist Convective Adjustment (MCA) scheme for deep convection simulates a single ITCZ over the SST maximum, for any of the SST forcings. This is consistent with the findings of earlier modeling studies which suggested that models with the MCA scheme tend to simulate a single ITCZ over the warmest SST (Lau et al. 1988; Hess et al. 1993; Lee et al. 2003). Judging from the dependence of the results on deep convection scheme used in these models, we can conclude that treatment of convective parameterization should be placed near the top of a list of model components whose modifications can affect the sensitivity of ITCZ to SST distribution. This is, of course, not surprising at all given that what we are investigating is the interaction between convection and dynamics. Similarly, treatment of dynamics may have a significant impact on sensitivity of ITCZ to SST. For example, the treatment of moisture advection, which has a profound impact on the moisture distribution as one of the input parameters for convective schemes, should also be placed near the top of a list, particularly, of those parameters that are influential on the vertical moisture advection (Rasch and Williamson 1991).

6. Concluding Remarks

Impact of meridional gradient of SST on the mean tropical circulation of the atmosphere in Aqua Planet Experiment (APE) simulations is analyzed to identify factors that control the latitudinal preference of the Inter Tropical Convergence Zone (ITCZ). In this study, ITCZ is defined by the maximum of zonally averaged total precipitation. The APE intercomparison results suggest that zonally averaged precipitation pattern and the formation and positioning of ITCZ are found to be strongly sensitive to meridional distribution of SST. The *Control* SST forcing with a narrow equatorial SST maximum yields a single ITCZ at the equatorial SST maximum. As the peak of the equatorial SST flattens, the single precipitation peak is gradually replaced by dual peaks flanking the

SST maximum. The spatial organization and the dynamics of convective structures are found to depend strongly on the meridional gradient of SST. While meridional SST gradient around the narrow SST peak in *Control* case favours a strong and single equatorial ITCZ in all the models, flat equatorial SST peak in *FLAT* case favours double ITCZs occurring at $0.2^{\circ}\text{C}/\text{deg}$ to $0.3^{\circ}\text{C}/\text{deg}$ SST gradient, flanking the SST maximum in the majority of the models. Although there is reasonable consistency in the SST sensitivity of ITCZ among the models in the *Control* case, there exists strong disparity among the models in *FLAT* case, in which some models still yield a dominant equatorial precipitation maximum. While the total and convective precipitation responses are consistent among the models for each of the SST forcings, the large-scale precipitation response shows considerable variations among them in *FLAT* case. The organization and positioning of the ITCZ are found to be primarily due to boundary layer moisture convergence related to the SST gradient. Furthermore, meridional gradient of temperature in the troposphere influenced by the underlying SST gradient is also found to be an important factor related to the positioning of ITCZ. The transition between the single and double ITCZ regimes occurs for *FLAT* SST variation, which is found to be similar to the observed mean SST distribution over the major monsoonal regions such as the Bay of Bengal and western Pacific Ocean during the summer season. Models that simulate double ITCZs in this case simulate an equatorial easterly jet in the upper troposphere about $\sim 13^{\circ}$ southward of the northern branch of double ITCZs. This seems analogous to the Tropical Easterly Jet (TEJ) observed southward of the northern branch of the double ITCZs over the Indian region in summer. This is a unique feature and important component of the Indian summer monsoon. In the particular models, the jet is in thermal wind balance with positive meridional temperature gradient vertically coherent almost in the entire depth of the troposphere, which is maintained by convective heating along the ITCZ strengthened by boundary-layer moisture convergence. TEJ is found to be in geostrophic balance.

Acknowledgments.

The authors are grateful to the APE modeling group for data provision. The authors also thank Dr. M. Hosaka and Dr. S. Yukimoto for their help in setting up the Aqua Planet version of the MRI model. KR was supported by the KAKUSHIN Program of the Ministry of Education, Culture, Sports, Science, and Technology (MEXT), Japan and by the research grant from Megha-Tropiques mission of ISRO.

References

- Adler, R. F., et al., 2003: The version-2 Global Precipitation Climatology Project (GPCP) monthly precipitation analysis (1979-present). *J. Hydrometeor.*, **4**, 1147–1167.
- Arakawa, A. and W. H. Schubert, 1974: Interaction of a cumulus cloud ensemble with the largescale environment. *J. Atmos. Sci.*, **31**, 674–701.
- Back, L. E. and C. S. Bretherton, 2009: On the relationship between SST gradients, boundary layer winds, and convergence over the Tropical Ocean. *J. Climate*, **97**, 4182–4196.
- Bjerknes, J., 1969: Atmospheric teleconnections from the Equatorial Pacific. *Mon. Wea. Rev.*, **97**, 163–172.
- Burpee, R. W., 1972: The origin and structure of easterly waves in the lower troposphere of North Africa. *J. Atmos. Sci.*, **29**, 77–90.
- Chao, W. C., 2000: Multiple quasi-equilibria of the ITCZ and the origin of monsoon onset. *J. Atmos. Sci.*, **57**, 641–652.
- Emanuel, K. A., 1991: A scheme for representing cumulus convection in large-scale models. *J. Atmos. Sci.*, **48**, 2313–2335.
- Gregory, D. and P. R. Rowntree, 1990: A mass flux convection scheme with representation of cloud ensemble characteristics and stability-dependent closure. *Mon.*

- Wea. Rev.*, **118**, 1483–1506.
- Hastenrath, S. and P. Lamb, 1977: Some aspects of circulation and climate over the eastern equatorial Atlantic. *Mon. Wea. Rev.*, **105**, 1019–1023.
- Hayashi, Y. and A. Sumi, 1986: The 30-40 day oscillations simulated in an aquaplanet model. *J. Meteor. Soc. Japan*, **64**, 451–466.
- Hess, P., D. Battisti, and P. Rasch, 1993: Maintenance of the intertropical convergence zones and the large-scale tropical circulation on a water-covered earth. *J. Atmos. Sci.*, **50**, 691–713.
- Koteswaram, P., 1958: The easterly jet stream in the tropics. *Tellus*, **10**, 43–57.
- Lau, N.-C., I. M. Held, and J. D. Neelin, 1988: The Madden-Julian oscillation in an idealized general circulation model. *J. Atmos. Sci.*, **45**, 3810–3832.
- Lee, M.-I., I.-S. Kang, and B. E. Mapes, 2003: Impacts of cumulus convection parameterization on aqua-planet AGCM simulations of tropical intraseasonal variability. *J. Meteor. Soc. Japan*, **81**, 963–992.
- Lietzke, C. E., C. Deser, and T. H. V. Haar, 2001: Evolutionary structure of the eastern Pacific double ITCZ based on satellite moisture profile retrievals. *J. Climate*, **14**, 743–751.
- Lindzen, R. S. and A. Hou, 1988: Hadley circulations for zonally averaged heating centered off the equator. *J. Atmos. Sci.*, **45**, 2416–2427.
- Lindzen, R. S. and S. Nigam, 1987: On the role of sea surface temperature gradients in forcing low-level winds and convergence in the tropics. *J. Atmos. Sci.*, **44**, 2418–2436.
- Lorant, V. and J. F. Royer, 2001: Sensitivity of equatorial convection to horizontal resolution in aqua-planet simulations with a variable resolution GCM. *Mon. Wea. Rev.*,

129, 2730–2745.

- Manabe, S., D. G. Hahn, and J. L. Holloway, 1974: The seasonal variation of the tropical circulation as simulated by a global model of the atmosphere. *J. Atmos. Sci.*, **31**, 43–83.
- Moorthi, S. and M. J. Suarez, 1992: Relaxed Arakawa-Schubert: A parameterization of moist convection for General Circulation models. *Mon. Wea. Rev.*, **120**, 978–1002.
- Neale, R. B. and B. J. Hoskins, 2000a: A standard test for AGCMs and their physical parameterizations. I: The proposal. *Atmos. Sci. Lett.*, **1**, 101–107.
- Neale, R. B. and B. J. Hoskins, 2000b: A standard test for AGCMs and their physical parameterizations. II: Results for the Met. office model. *Atmos. Sci. Lett.*, **1**, 108–114.
- Numaguti, A., 1993: Dynamics and energy balance of the Hadley circulation and the tropical precipitation zones: Significance of the distribution of evaporation. *J. Atmos. Sci.*, **50**, 1874–1887.
- Numaguti, A. and Y.-Y. Hayashi, 1991a: Behavior of cumulus activity and the structures of circulations in a ‘aqua-planet’ model. Part I: The structure of the super clusters. *J. Meteor. Soc. Japan*, **69**, 541–561.
- Numaguti, A. and Y.-Y. Hayashi, 1991b: Behavior of cumulus activity and the structures of circulations in a ‘aqua-planet’ model. Part II: Eastward moving planetary scale structure and the intertropical convergence zone. *J. Meteor. Soc. Japan*, **69**, 563–579.
- Ose, T., T. Tokioka, and K. Yamazaki, 1989: Hadley circulation and penetrative cumulus convection. *J. Meteor. Soc. Japan*, **67**, 605–619.
- Pan, D. M. and D. A. Randall, 1998: A cumulus parameterization with a prognostic closure. *Quart. J. Roy. Meteor. Soc.*, **124**, 949–981.

- Pike, A. C., 1971: Intertropical convergence zone studied with an interacting atmosphere and ocean model. *Mon. Wea. Rev.*, **99**, 469–477.
- Ramage, C. S., 1974: Structure of an oceanic near-equatorial trough deduced from research aircraft traverses. *Mon. Wea. Rev.*, **102**, 754–759.
- Rasch, P. J. and D. L. Williamson, 1991: The sensitivity of a general circulation model climate to the moisture transport formulation. *J. Geophys. Res.*, **96**, 13 123–13 137.
- Rayner, N. A., D. E. Parker, E. B. Horton, C. K. Folland, L. V. Alexander, D. P. Rowell, E. C. Kent, and A. Kaplan, 2003: Global analyses of SST, sea ice and night marine air temperature since the late nineteenth century. *J. Geophys. Res.*, **108**, doi:10.1029/2002JD002 670.
- Sadler, J. C., 1975: The monsoon circulation and cloudiness over the GATE area. *Mon. Wea. Rev.*, **103**, 369–387.
- Srinivasan, J., 2001: A simple thermodynamic model for seasonal variation of monsoon rainfall. *Curr. Sci.*, **80**, 73–77.
- Srinivasan, J., 2003: Diagnostic study of errors in the simulation of tropical continental precipitation in general circulation models. *Annales Geophys.*, **21**, 1197–1207.
- Sumi, A., 1992: Pattern formation of convective activity over the aqua-planet with globally uniform sea surface temperature (SST). *J. Meteor. Soc. Japan*, **70**, 855–876.
- Swinbank, R., T. N. Palmer, and M. K. Davey, 1988: Numerical simulations of the Madden and Julian Oscillation. *J. Atmos. Sci.*, **45**, 774–788.
- Thorncroft, C. D. and M. Blackburn, 1999: Maintenance of the African easterly jet. *Quart. J. Roy. Meteor. Soc.*, **125**, 763–786.

- Tiedtke, M., 1989: A comprehensive mass flux scheme for cumulus parameterization in large-scale models. *Mon. Wea. Rev.*, **117**, 1779–1800.
- Uppala, S. M., P. W. Kallberg, A. J. Simmons, and Co-authors, 2005: The ERA-40 Reanalysis. *Quart. J. Roy. Meteor. Soc.*, **131**, 2961–3012.
- Waliser, D. E. and R. C. J. Somerville, 1994: The preferred latitudes of the intertropical convergence zone. *J. Atmos. Sci.*, **51**, 1619–1639.
- Zhang, G. J. and N. A. McFarlane, 1995: Role of convective scale momentum transport in climate simulation. *J. Geophys. Res.*, **100**, 1417–1426.

List of Figures

- FIG. 1. Latitudinal variation of SST (dashed curve), and its meridional gradient (solid curve) and second derivative (dotted curve) assigned for (a) *Control*, (b) *Q_{obs}* and (c) *FLAT* distributions. SST gradient with absolute values between $0.2^{\circ}\text{C}=\text{deg}$ and $0.3^{\circ}\text{C}=\text{deg}$ are highlighted.
- FIG. 2. Latitudinal variation of zonally averaged total precipitation for (a) *Control*, (b) *Q_{obs}* and (c) *FLAT* simulations by individual APE models (as indicated). For *FLAT* SST forcing, total precipitation of 4 mm/day is highlighted.
- FIG. 3. Latitudinal variation of zonally averaged precipitation minus evaporation ($P-E$) for (a) *Control* and (b) *FLAT* (zero value is highlighted) simulations by individual APE models (as indicated).
- FIG. 4. Latitudinal variation of zonally averaged convective precipitation for (a) *Control* and (b) *FLAT* simulations by individual APE models (as indicated).

FIG. 5. Latitudinal variation of zonally averaged large-scale precipitation for (a) *Control* and (b) *FLAT* simulations by individual APE models (as indicated).

FIG. 6. Latitudinal variation of zonally averaged $P-E$ (dashed) and vertically integrated specific humidity (solid) taken from simulations by three representative models of the two categories of APE models, with *Control* (blue) and *FLAT* (red) SST forcings.

FIG. 7. Latitudinal variation of zonally averaged $q \frac{\partial V}{\partial y}$ simulated by the MRI model with *Control* (upper) and *FLAT* (lower) SST forcings.

FIG. 8. As in Fig. 6, but for latitudinal variation of zonally averaged $P-E$ (dashed) and vertically integrated lower level (1000-700 hPa) moisture convergence (solid) from *Control* (blue) and *FLAT* (red) simulations by selected models (as indicated).

FIG. 9. Latitudinal variation of zonally averaged difference in temperature relative to the temperature at the equator at 850 hPa (left) and 200 hPa (right) for *Control* (upper) and *FLAT* (lower) simulations by the individual APE models (as indicated).

FIG. 10. Latitude-height cross section of zonally averaged $\frac{\partial T}{\partial y}$ from *Control* (upper) and *FLAT* (lower) simulations by the (left) AGU and (right) MRI models.

FIG. 11. Latitudinal variation of zonally averaged zonal wind velocity (colored as indicated below the panel) and meridional circulation (v,w) (arrows with reference vector shown below) for simulations of the first category models (a) ECMWF, (b) MRI and for (c) NCAR with *Control* (left) and *FLAT* (right) SST forcings.

FIG. 12. Latitudinal variations of SST used for APE *Control* and *FLAT* simulations and those of observed SST (HadISST) averaged over oceanic domains of the Bay of Bengal (BoB; 80° - $100^{\circ}E$), western Pacific (WPac; 140° - $160^{\circ}E$) and Atlantic (Atl; 325° - $345^{\circ}E$).

FIG. 13. July climatologies (1980-2000) of (a) GPCP precipitation (white dashed contours for 4 mm/day and 8 mm/day), 150-hPa zonal wind speed (colored as indicated below the panel) and streamlines based on the ERA-40 reanalysis in the tropics. (b) Meridional cross section of July climatology of zonal wind velocity (colored as indicated below the panel) at 70_E based on ERA-40.

FIG. 14. Meridional sections of zonally averaged zonal wind velocity (left) and the zonal component of geostrophic wind (right) simulated in the MRI model with the *Control* (upper) and *FLAT* (lower) SST profiles.

List of Tables

TABLE 1. Specifics of the APE models analyzed in this study.

TABLE 2. Three latitudinal SST profiles for the APE simulations analyzed in this study.

List of Figures

1	Latitudinal variation of SST (dashed curve), and its meridional gradient (solid curve) and second derivative (dotted curve) assigned for (a) <i>Control</i> , (b) Q_{obs} and (c) <i>FLAT</i> distributions. SST gradient with absolute values between $0.2^{\circ}\text{C}/\text{deg}$ and $0.3^{\circ}\text{C}/\text{deg}$ are highlighted.	4
2	Latitudinal variation of zonally averaged total precipitation for (a) <i>Control</i> , (b) Q_{obs} and (c) <i>FLAT</i> simulations by individual APE models (as indicated). For <i>FLAT</i> SST forcing, total precipitation of 4 mm/day is highlighted.	5
3	Latitudinal variation of zonally averaged precipitation minus evaporation ($P - E$) for (a) <i>Control</i> and (b) <i>FLAT</i> (zero value is highlighted) simulations by individual APE models (as indicated).	6
4	Latitudinal variation of zonally averaged convective precipitation for (a) <i>Control</i> and (b) <i>FLAT</i> simulations by individual APE models (as indicated).	7
5	Latitudinal variation of zonally averaged large-scale precipitation for (a) <i>Control</i> and (b) <i>FLAT</i> simulations by individual APE models (as indicated).	8
6	Latitudinal variation of zonally averaged $P - E$ (dashed) and vertically integrated specific humidity (solid) taken from simulations by three representative models of the two categories of APE models, with <i>Control</i> (blue) and <i>FLAT</i> (red) SST forcings.	9
7	Latitudinal variation of zonally averaged $q\frac{\partial V}{\partial y}$ simulated by the MRI model with <i>Control</i> (upper) and <i>FLAT</i> (lower) SST forcings.	10

8	As in Fig. 6, but for latitudinal variation of zonally averaged $P - E$ (dashed) and vertically integrated lower level (1000-700 hPa) moisture convergence (solid) from <i>Control</i> (blue) and <i>FLAT</i> (red) simulations by selected models (as indicated).	11
9	Latitudinal variation of zonally averaged difference in temperature relative to the temperature at the equator at 850 hPa (left) and 200 hPa (right) for <i>Control</i> (upper) and <i>FLAT</i> (lower) simulations by the individual APE models (as indicated).	12
10	Latitude-height cross section of zonally averaged $\frac{\partial T}{\partial y}$ from <i>Control</i> (upper) and <i>FLAT</i> (lower) simulations by the (left) AGU and (right) MRI models.	13
11	Latitudinal variation of zonally averaged zonal wind velocity (colored as indicated below the panel) and meridional circulation (v, ω) (arrows with reference vector shown below) for simulations of the first category models (a) ECMWF, (b) MRI and for (c) NCAR with <i>Control</i> (left) and <i>FLAT</i> (right) SST forcings.	14
12	Latitudinal variations of SST used for APE <i>Control</i> and <i>FLAT</i> simulations and those of observed SST (HadISST) averaged over oceanic domains of the Bay of Bengal (BoB; $80^\circ - 100^\circ E$), western Pacific (WPac; $140^\circ - 160^\circ E$) and Atlantic (Atl; $325^\circ - 345^\circ E$).	15
13	July climatologies (1980-2000) of (a) GPCP precipitation (white dashed contours for 4 mm/day and 8 mm/day), 150-hPa zonal wind speed (colored as indicated below the panel) and streamlines based on the ERA-40 reanalysis in the tropics. (b) Meridional cross section of July climatology of zonal wind velocity (colored as indicated below the panel) at $70^\circ E$ based on ERA-40.	16

14 Meridional sections of zonally averaged zonal wind velocity (left) and the zonal component of geostrophic wind (right) simulated in the MRI model with the *Control* (upper) and *FLAT* (lower) SST profiles. 17

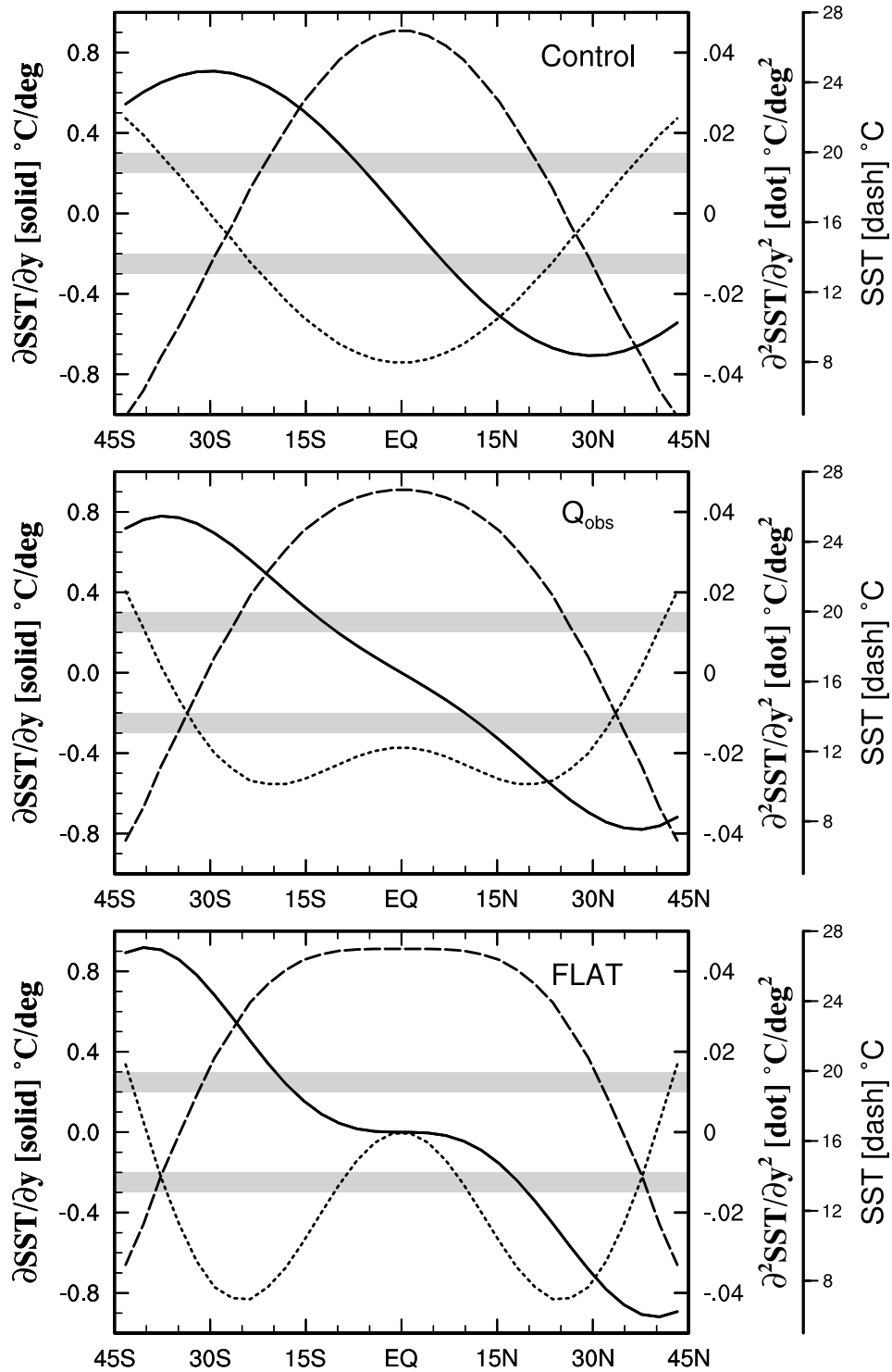


FIG. 1. Latitudinal variation of SST (dashed curve), and its meridional gradient (solid curve) and second derivative (dotted curve) assigned for (a) *Control*, (b) Q_{obs} and (c) *FLAT* distributions. SST gradient with absolute values between $0.2^{\circ}C/deg$ and $0.3^{\circ}C/deg$ are highlighted.

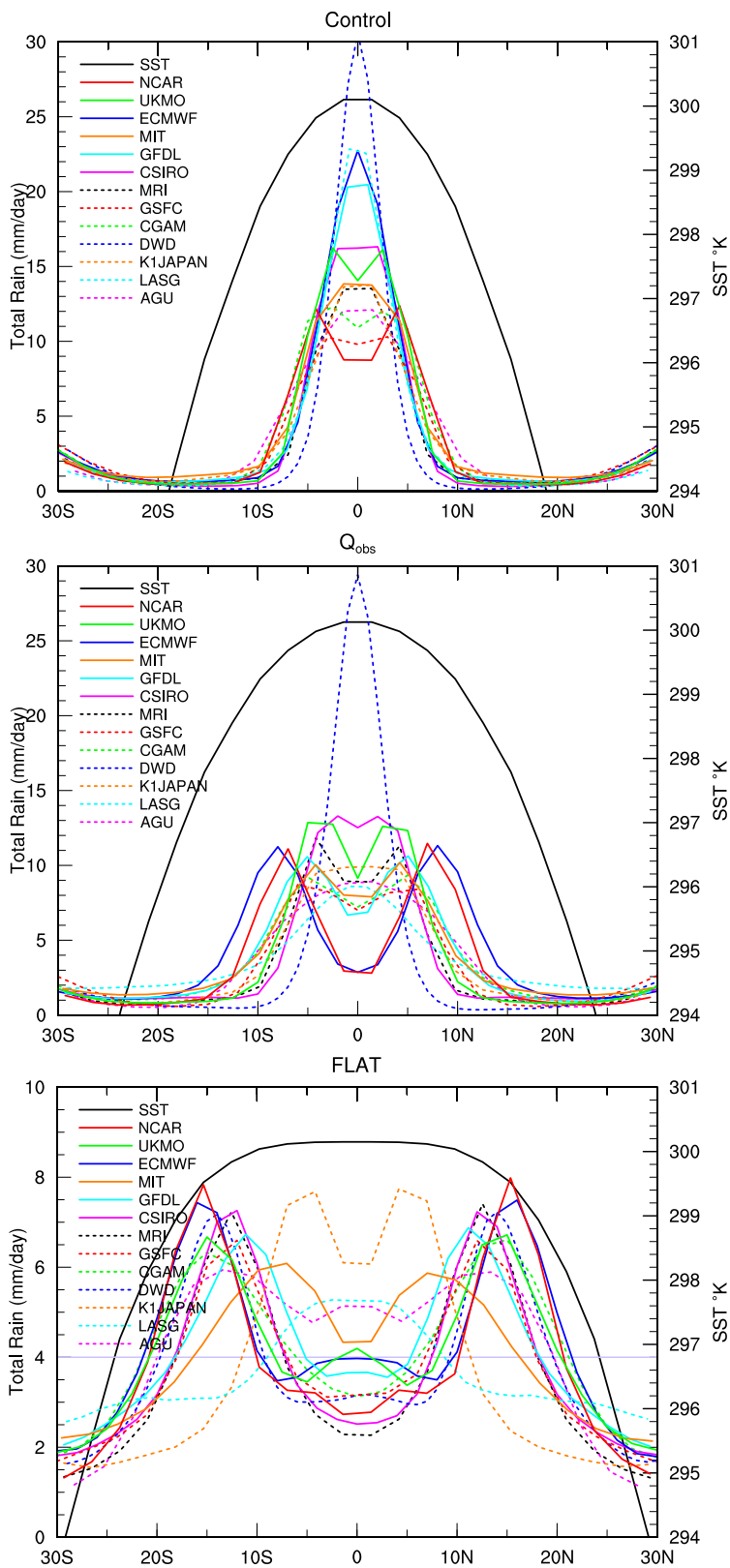


FIG. 2. Latitudinal variation of zonally averaged total precipitation for (a) *Control*, (b) Q_{obs} and (c) *FLAT* simulations by individual APE models (as indicated). For *FLAT* SST forcing, total precipitation of 4 mm/day is highlighted.

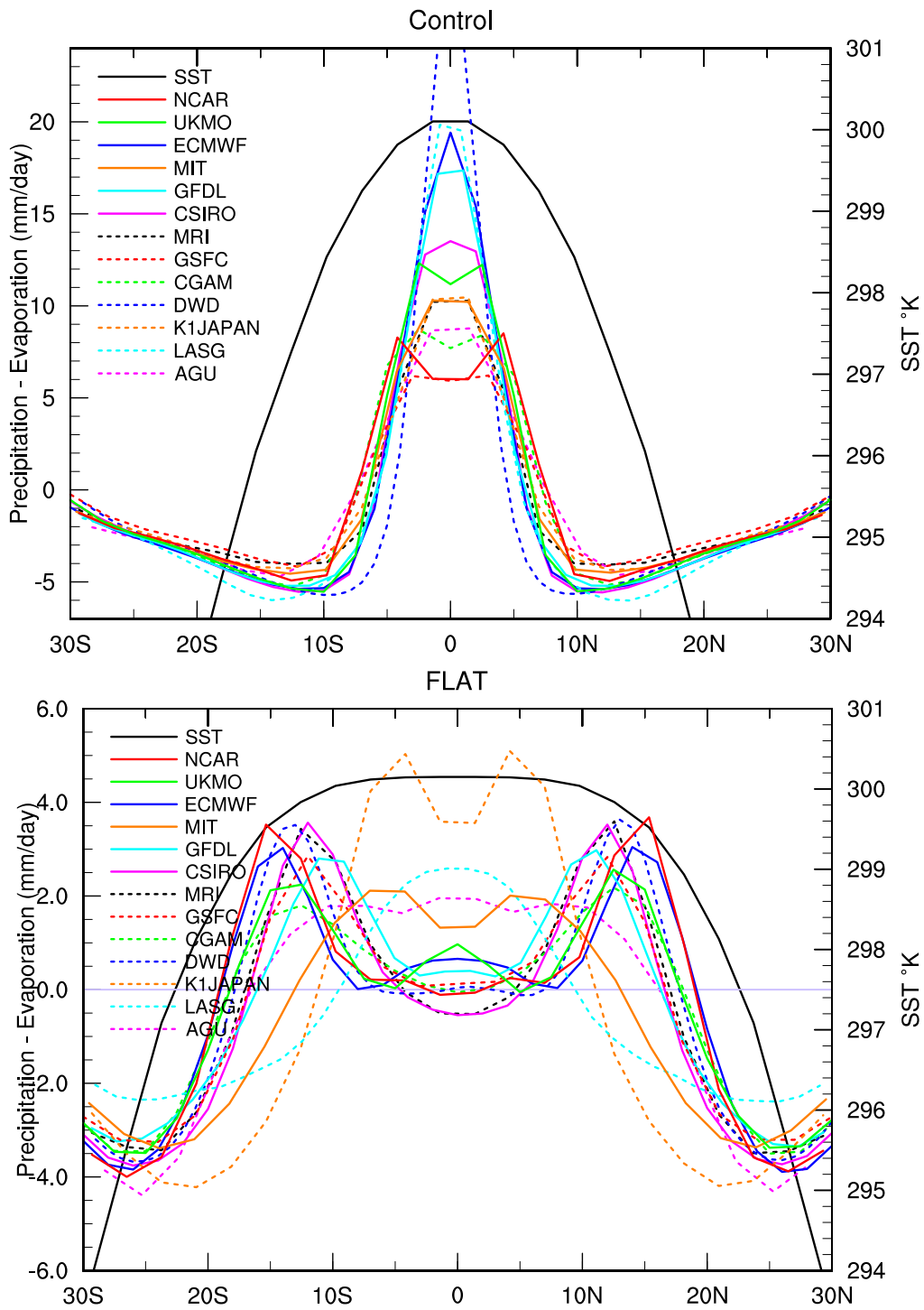


FIG. 3. Latitudinal variation of zonally averaged precipitation minus evaporation ($P - E$) for (a) *Control* and (b) *FLAT* (zero value is highlighted) simulations by individual APE models (as indicated).

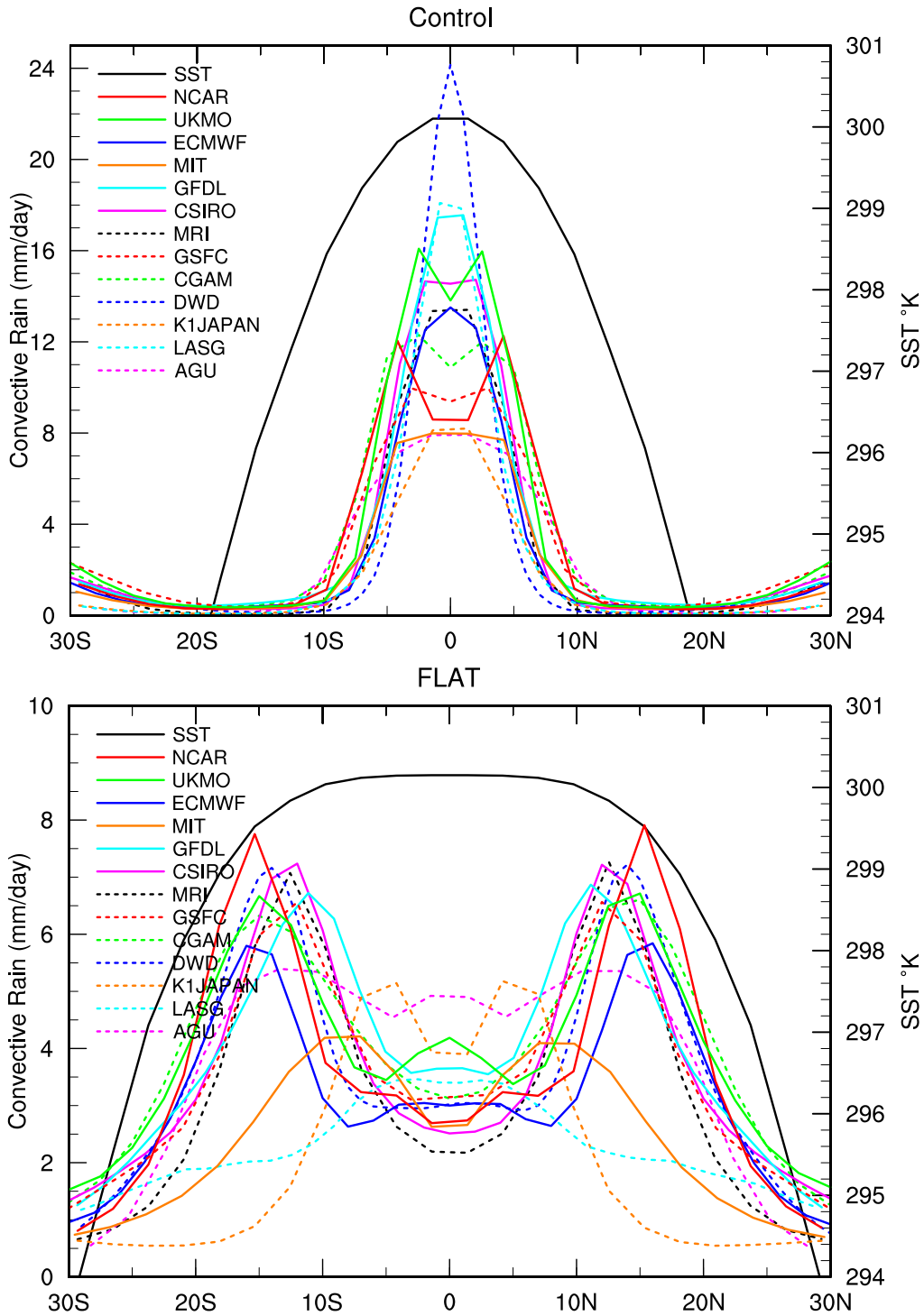


FIG. 4. Latitudinal variation of zonally averaged convective precipitation for (a) *Control* and (b) *FLAT* simulations by individual APE models (as indicated).

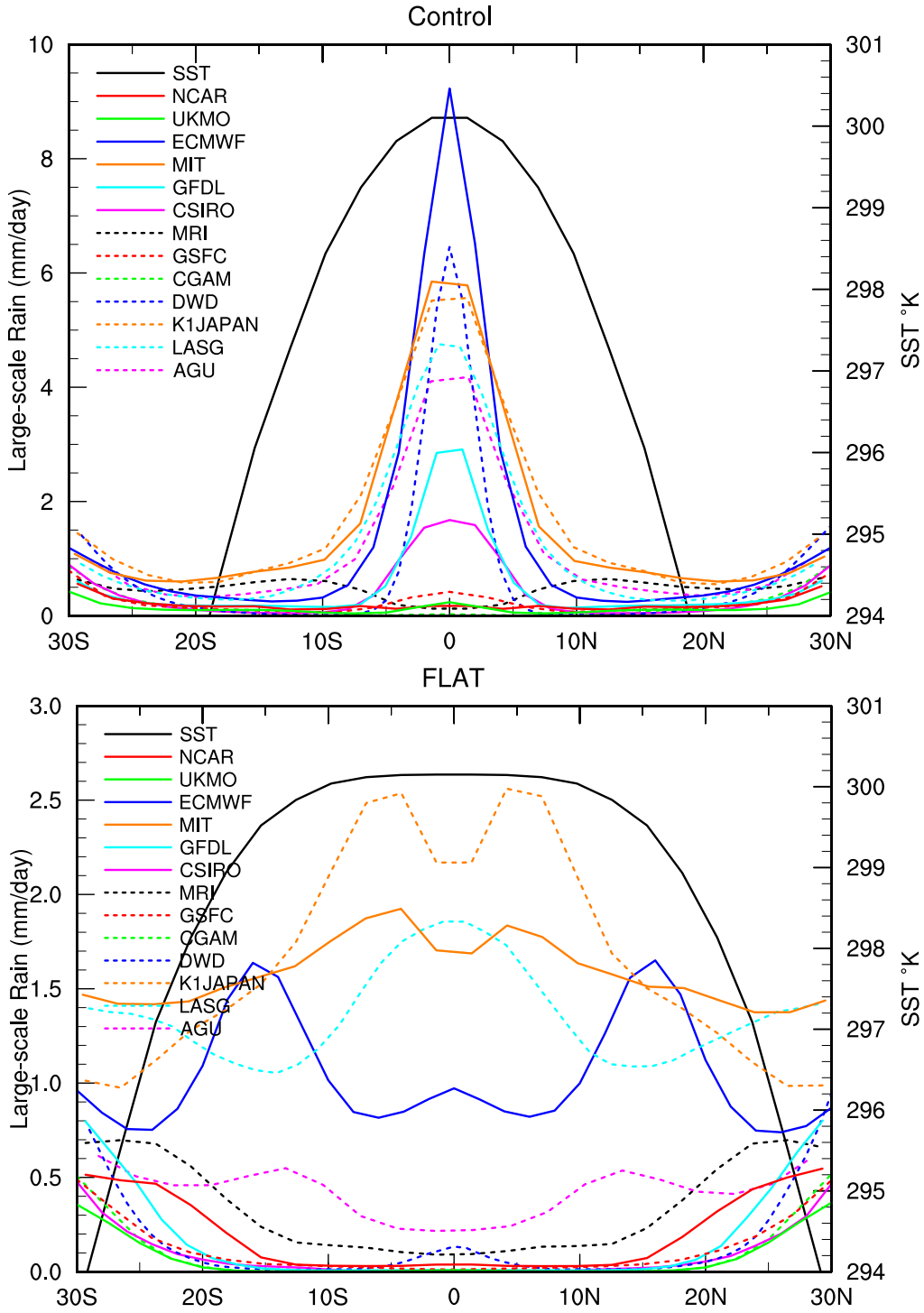


FIG. 5. Latitudinal variation of zonally averaged large-scale precipitation for (a) *Control* and (b) *FLAT* simulations by individual APE models (as indicated).

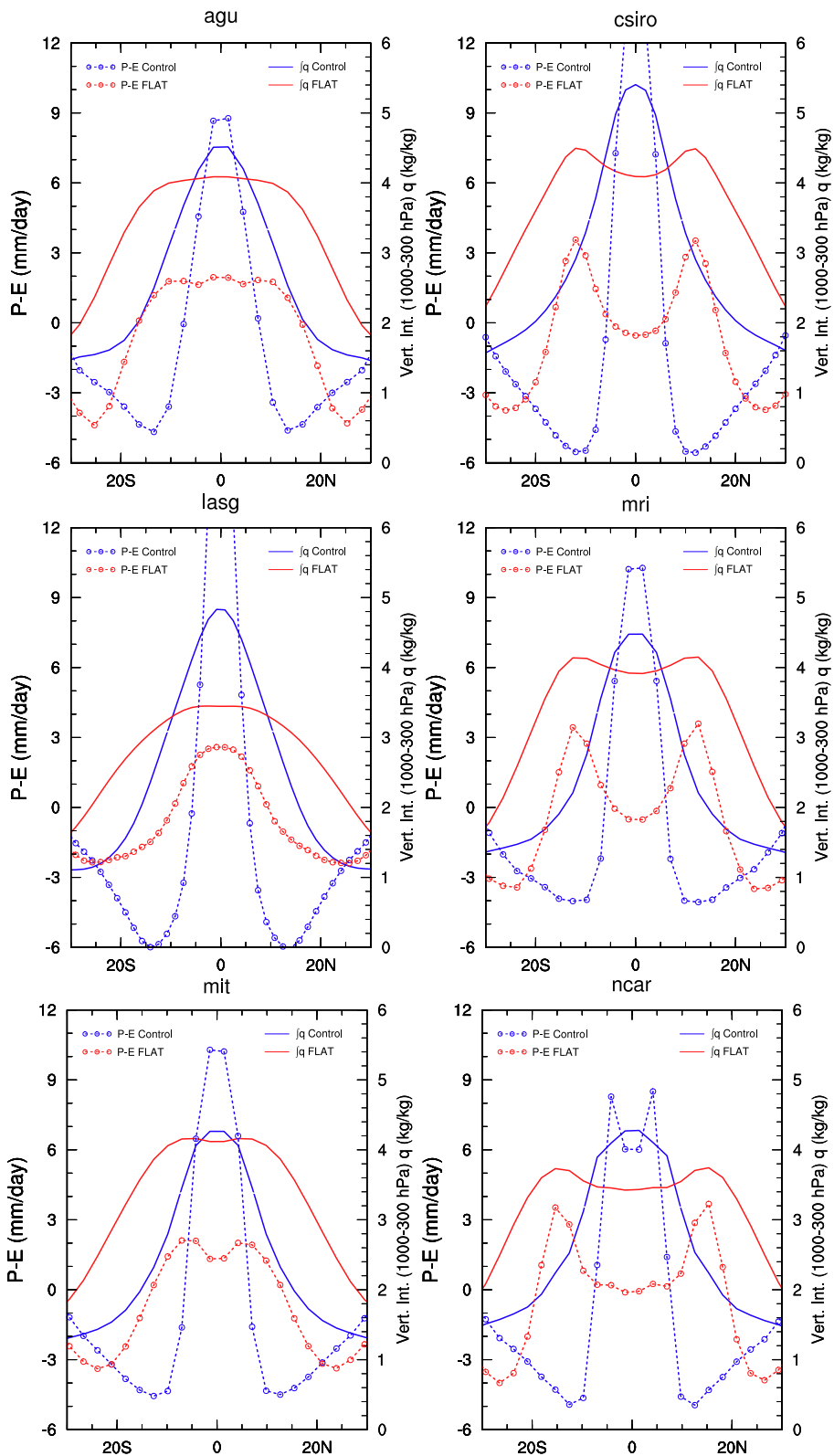


FIG. 6. Latitudinal variation of zonally averaged $P - E$ (dashed) and vertically integrated specific humidity (solid) taken from simulations by three representative models of the two categories of APE models, with *Control* (blue) and *FLAT* (red) SST forcings.

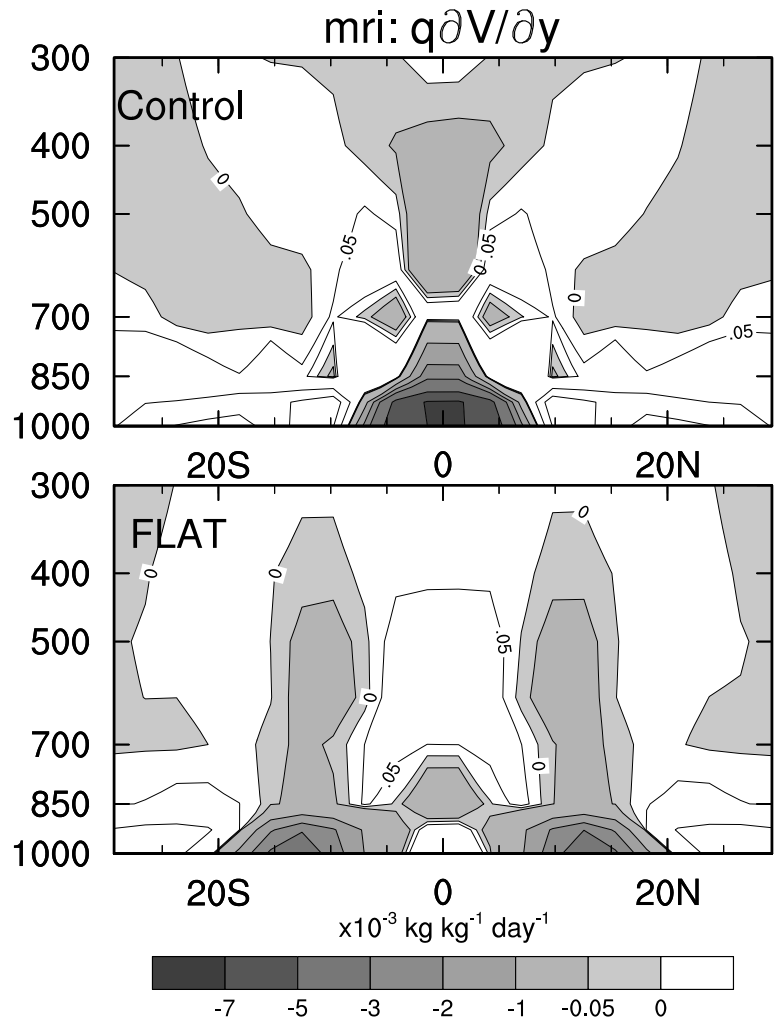


FIG. 7. Latitudinal variation of zonally averaged $q \frac{\partial V}{\partial y}$ simulated by the MRI model with *Control* (upper) and *FLAT* (lower) SST forcings.

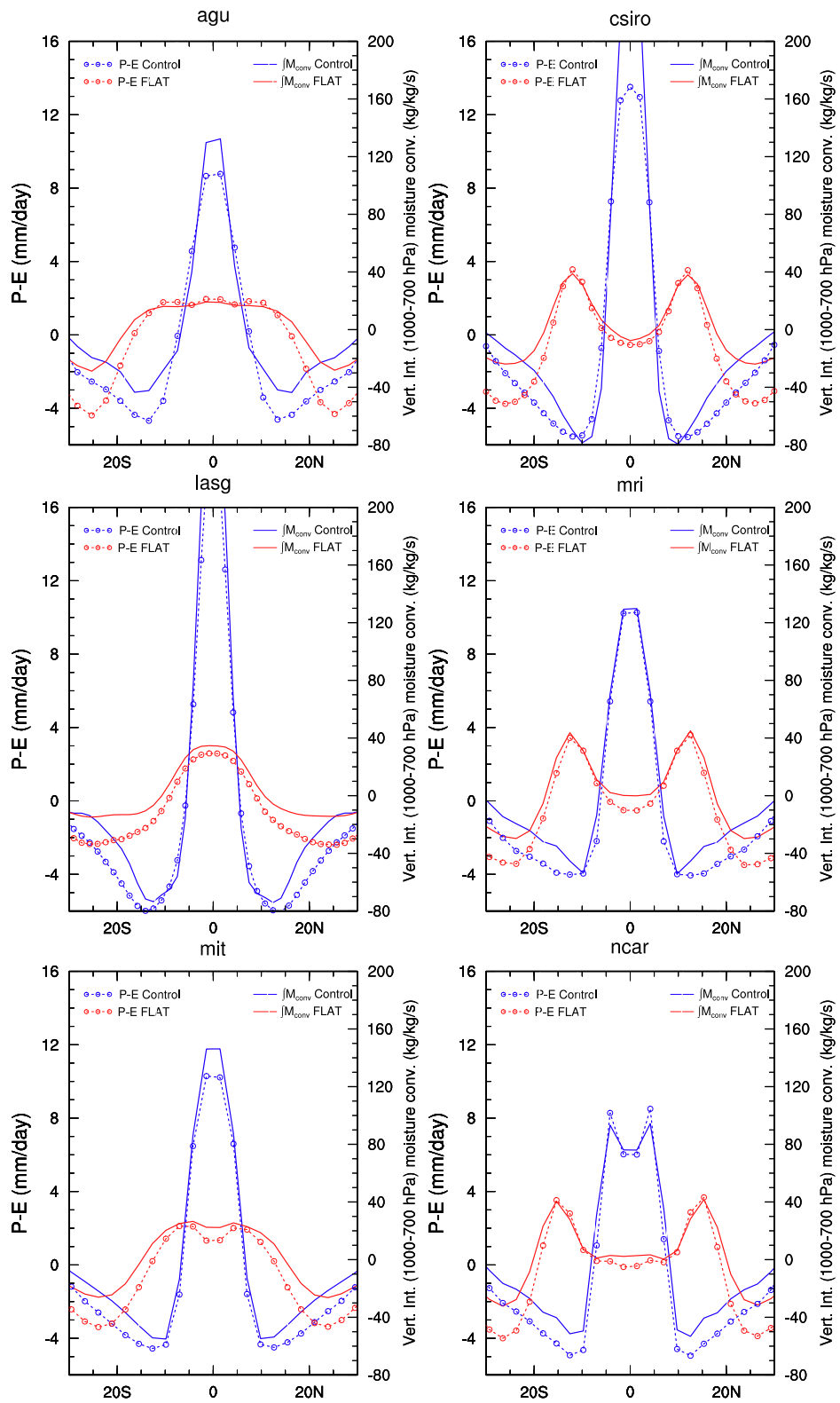


FIG. 8. As in Fig. 6, but for latitudinal variation of zonally averaged $P - E$ (dashed) and vertically integrated lower level (1000-700 hPa) moisture convergence (solid) from *Control* (blue) and *FLAT* (red) simulations by selected models (as indicated).

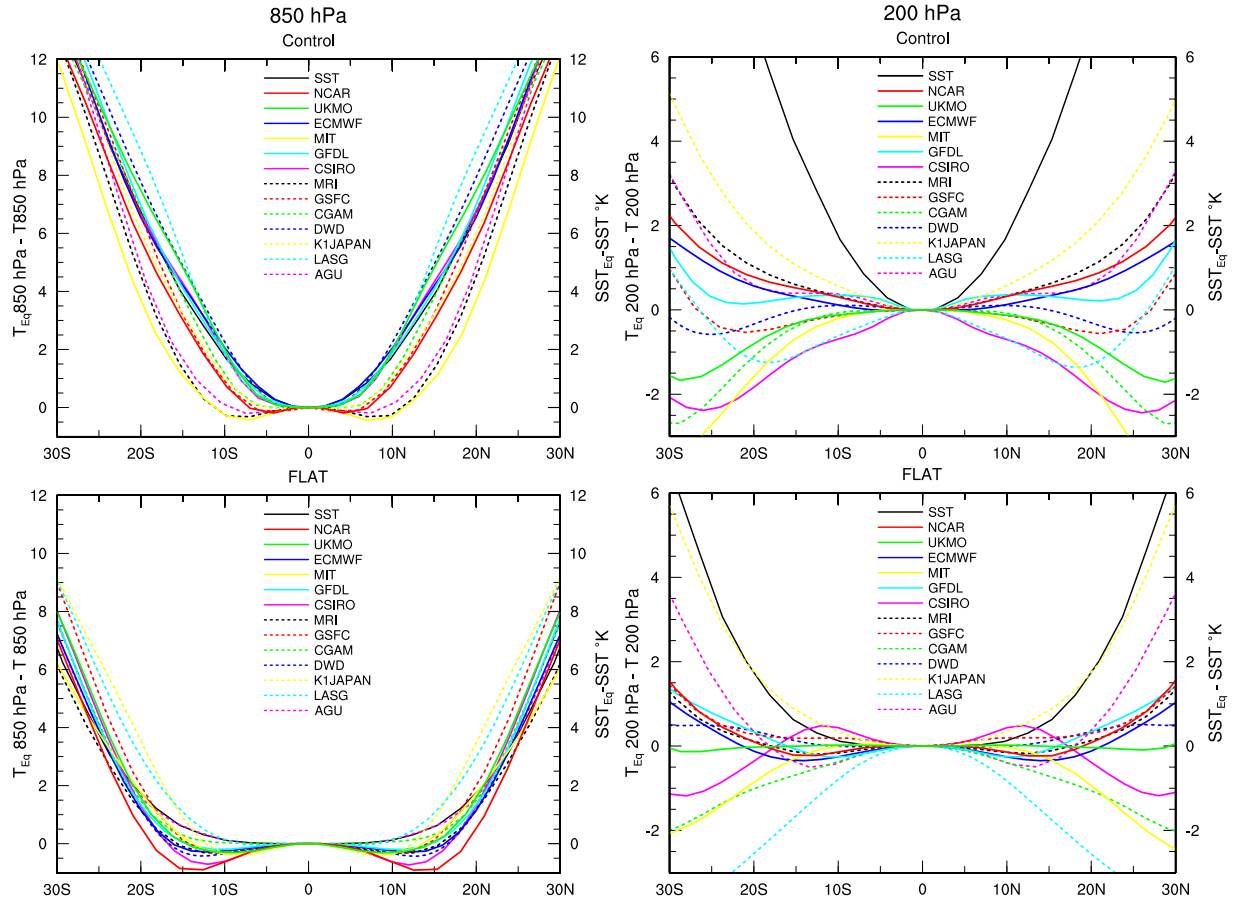


FIG. 9. Latitudinal variation of zonally averaged difference in temperature relative to the temperature at the equator at 850 hPa (left) and 200 hPa (right) for *Control* (upper) and *FLAT* (lower) simulations by the individual APE models (as indicated).

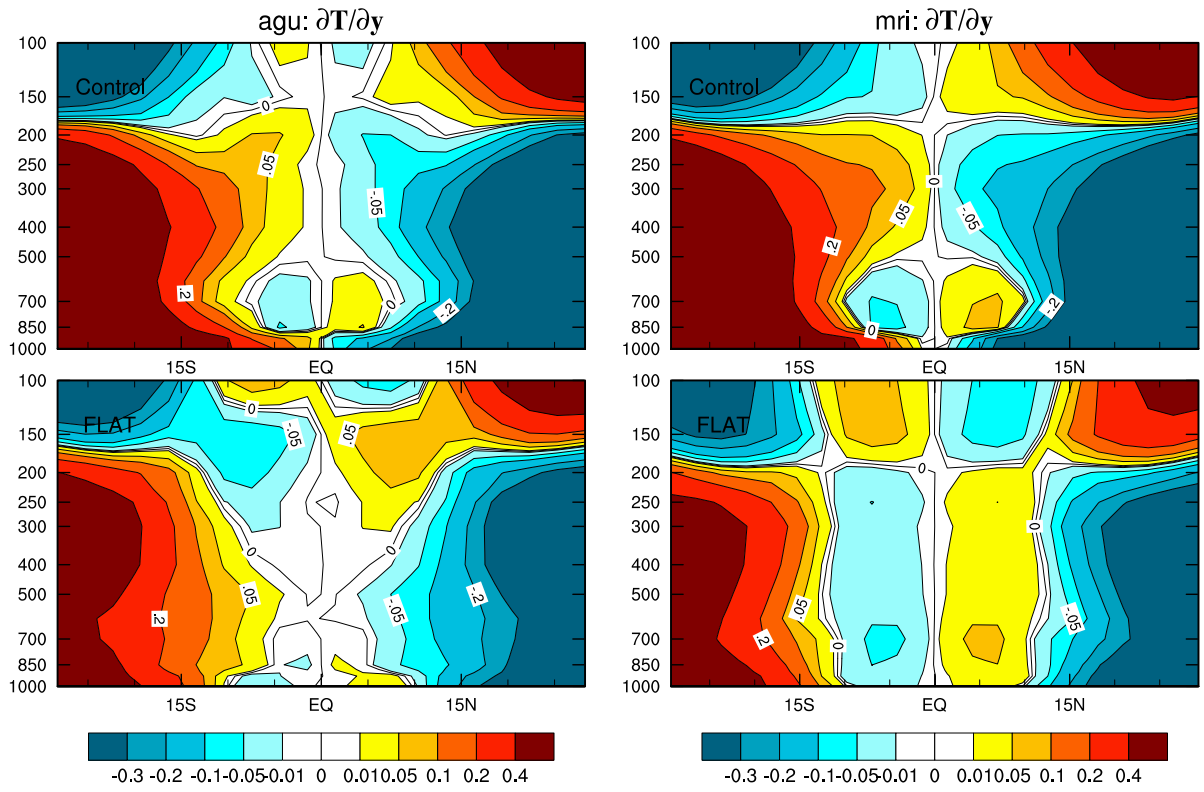


FIG. 10. Latitude-height cross section of zonally averaged $\frac{\partial T}{\partial y}$ from *Control* (upper) and *FLAT* (lower) simulations by the (left) AGU and (right) MRI models.

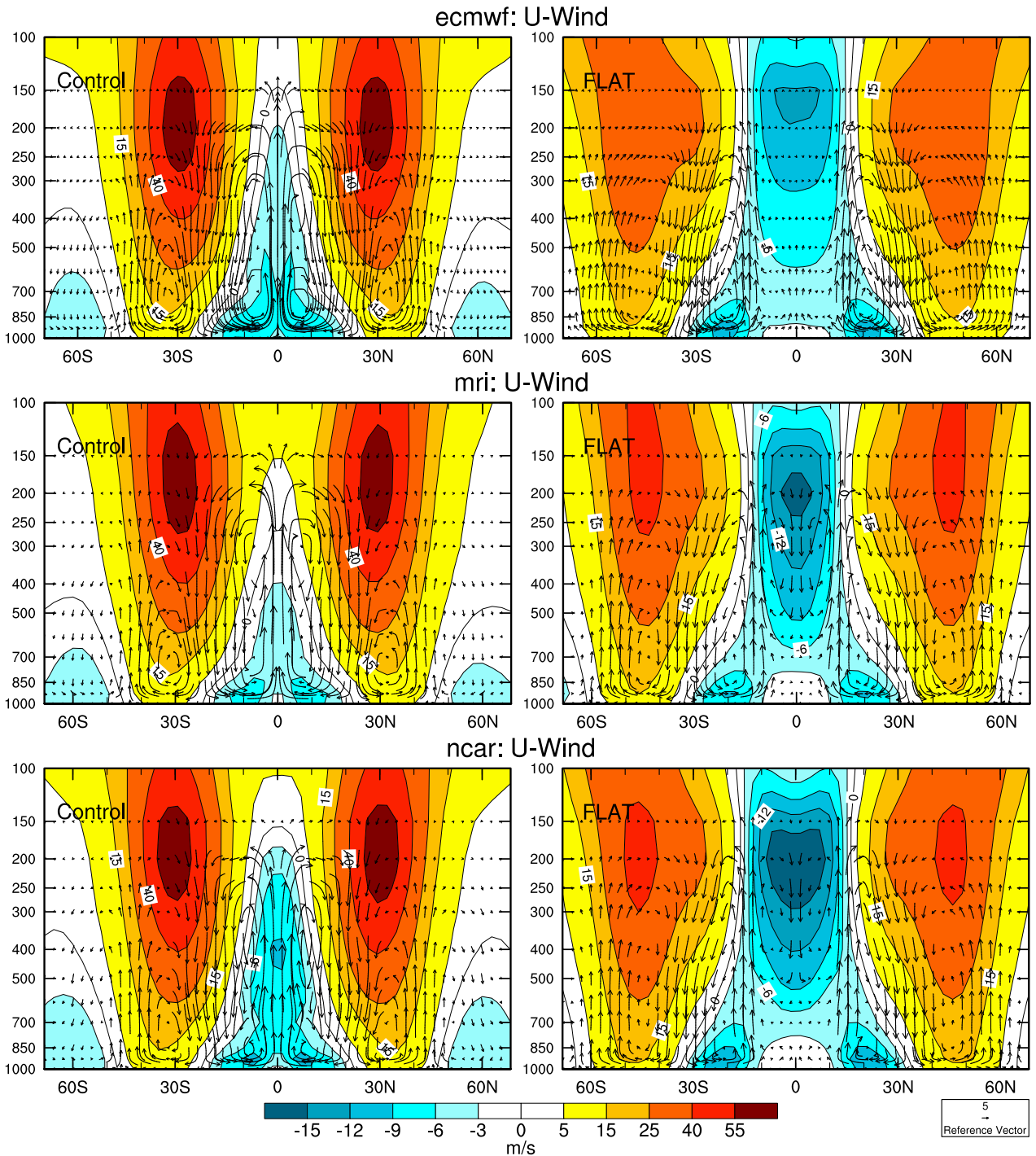


FIG. 11. Latitudinal variation of zonally averaged zonal wind velocity (colored as indicated below the panel) and meridional circulation (v, ω) (arrows with reference vector shown below) for simulations of the first category models (a) ECMWF, (b) MRI and for (c) NCAR with *Control* (left) and *FLAT* (right) SST forcings.

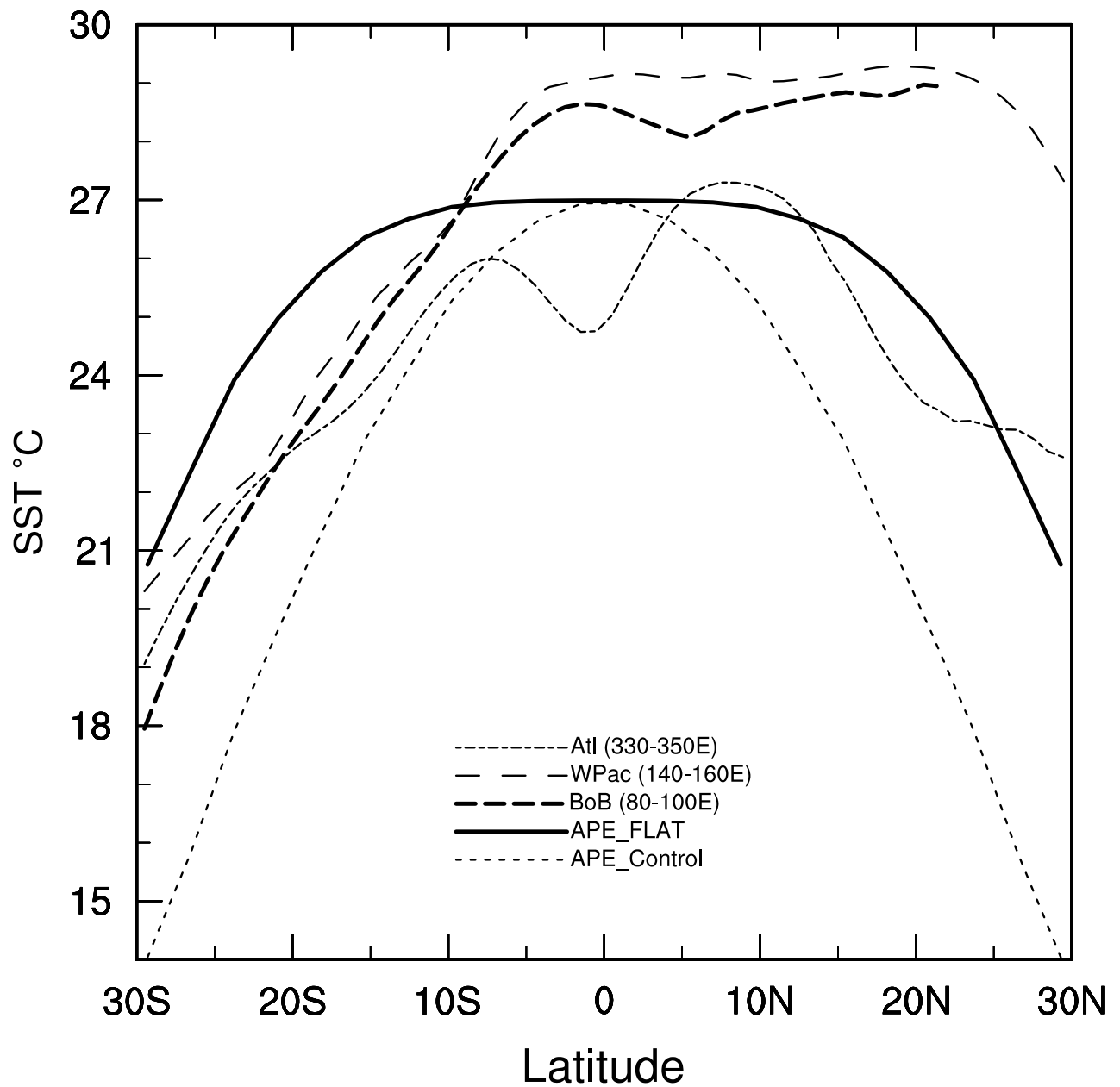


FIG. 12. Latitudinal variations of SST used for APE *Control* and *FLAT* simulations and those of observed SST (HadISST) averaged over oceanic domains of the Bay of Bengal (BoB; 80° – 100°E), western Pacific (WPac; 140° – 160°E) and Atlantic (Atl; 325° – 345°E).

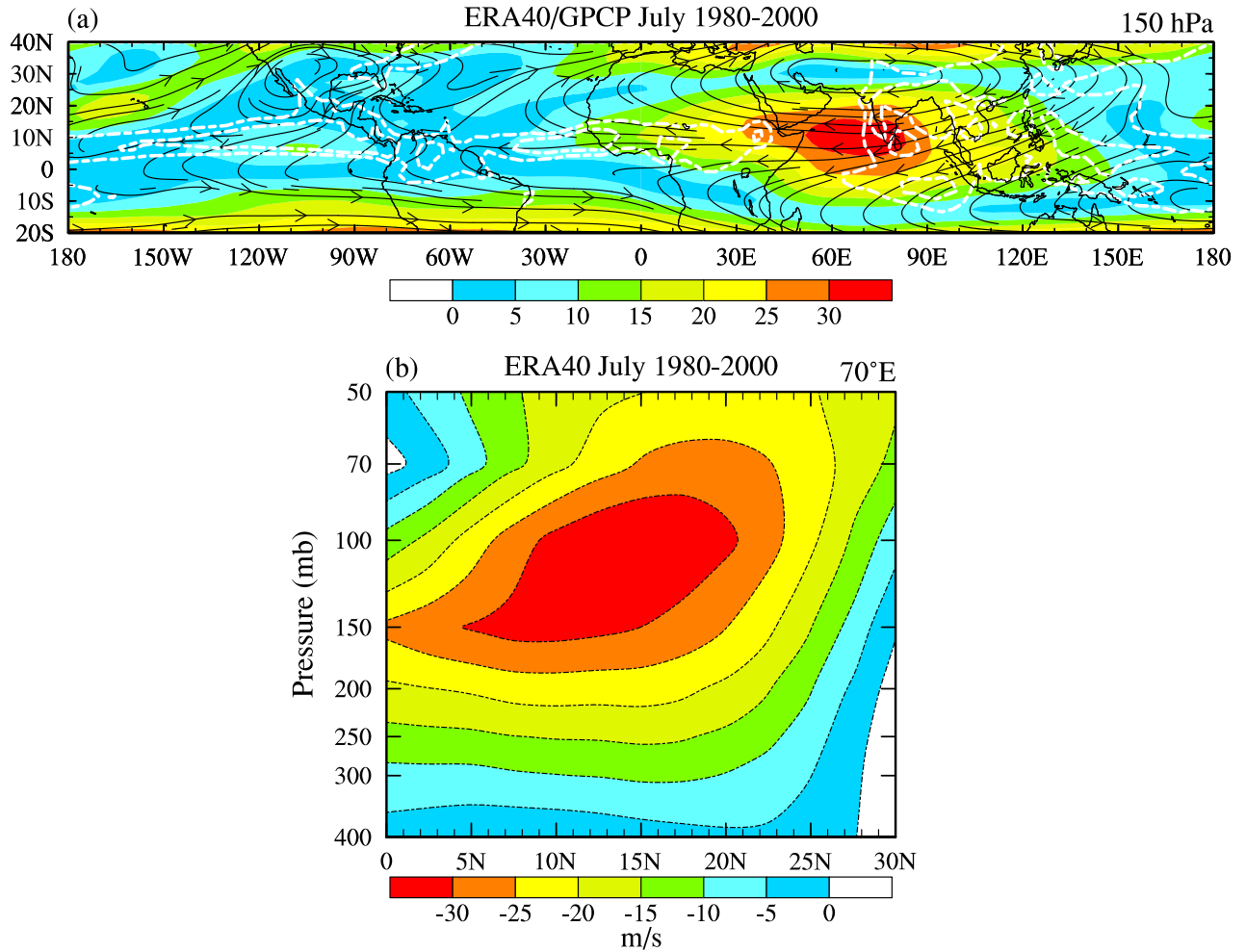


FIG. 13. July climatologies (1980-2000) of (a) GPCP precipitation (white dashed contours for 4 mm/day and 8 mm/day), 150-hPa zonal wind speed (colored as indicated below the panel) and streamlines based on the ERA-40 reanalysis in the tropics. (b) Meridional cross section of July climatology of zonal wind velocity (colored as indicated below the panel) at 70°E based on ERA-40.

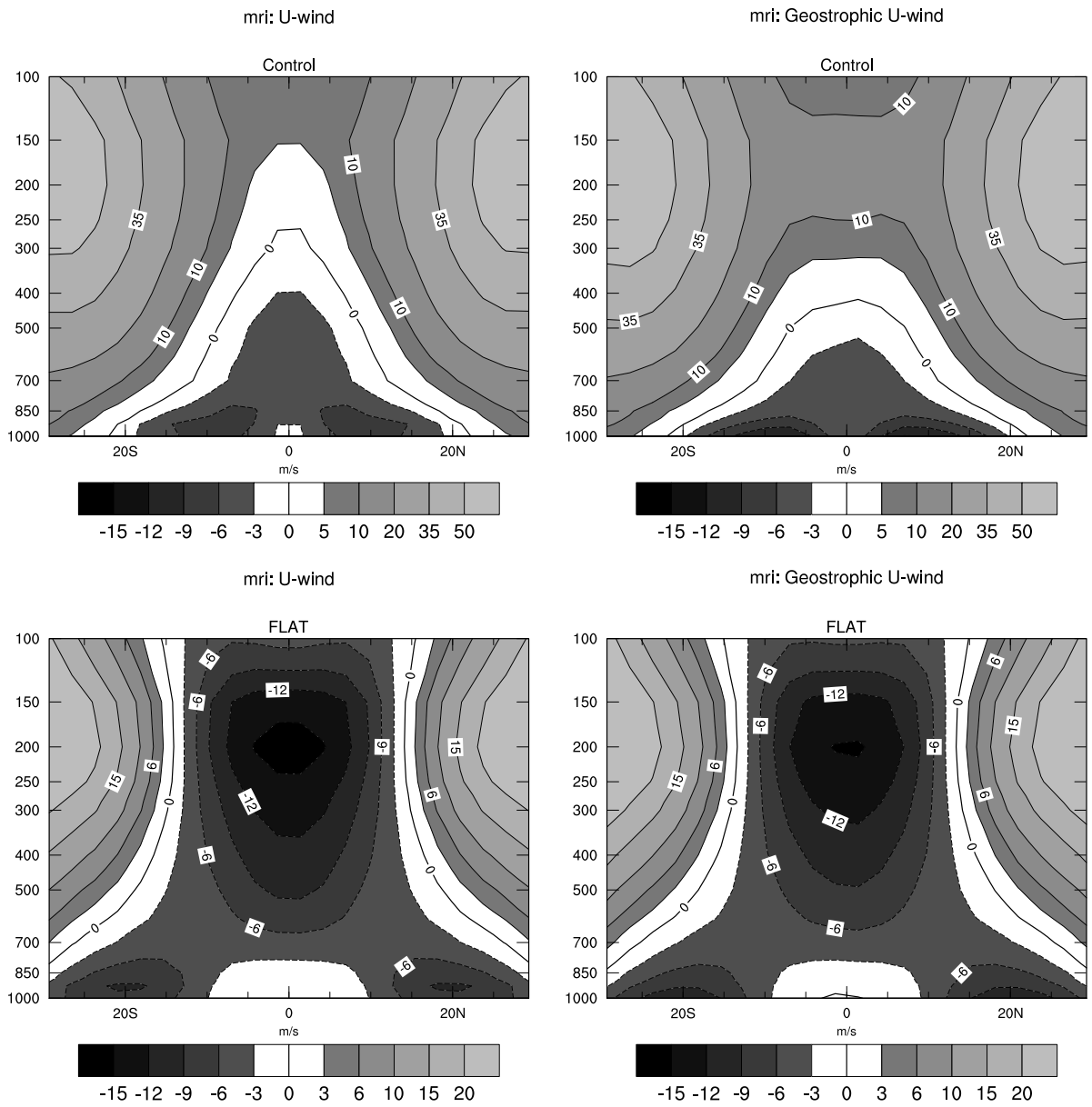


FIG. 14. Meridional sections of zonally averaged zonal wind velocity (left) and the zonal component of geostrophic wind (right) simulated in the MRI model with the *Control* (upper) and *FLAT* (lower) SST profiles.

List of Tables

1	Specifics of the APE models analyzed in this study.	19
2	Three latitudinal SST profiles for the APE simulations analyzed in this study. . . .	20

TABLE 1. Specifics of the APE models analyzed in this study.

APE Models	Dynamics	Deep convection	Closure/Trigger
AGU (Japan) T39L48 (3×2.8)	Spectral Eulerian	?	CAPE
CGAM (UK) N48L30 (3.75×2.5)	Arakawa B grid	?	Cloud base buoyancy
CSIRO (Australia) C48L18 (2×2)	Conformal cubic grid Semi-lagrangian	CSIRO mass-flux scheme	Cloud base mass flux
DWD (Germany) ni=64 L31 (1.25×1.25)	icosahedral-hexagonal grid	?	CAPE Moisture Convergence
ECMWF (UK) T _L 159L60 (2×2)	Spectral Semi-lagrangian	?	CAPE Moisture convergence
GFDL (USA) N72L24 (2.5×2)	Arakawa B grid	Relaxed Arakawa-Schubert (?)	CAPE/Threshold
GSFC (USA) N48 L34 (3.75×3)	4th order global grid	Relaxed Arakawa-Schubert (?)	CAPE/Threshold
K1-JAPAN T42L20	Spectral s-l moisture and cloud	Prognostic Arakawa-Schubert (?)	CAPE Relative humidity
LASG (China) R42L9 (2.825×1.6)	Spectral Eulerian	MCA	Moist Convective Instability
MIT (USA) C32L30	280 km cubed sphere	Relaxed Arakawa-Schubert (?)	CAPE/Threshold
MRI (Japan) T42L30	Spectral Eulerian	Prognostic Arakawa-Schubert (?)	CAPE Relative humidity
NCAR (USA) T42L26	Spectral Eulerian	?	CAPE
UKMO (UK) N48L30 (3.75×2.5)	Arakawa C grid	?	Cloud base buoyancy

TABLE 2. Three latitudinal SST profiles for the APE simulations analyzed in this study.

Case	SST Distribution
<i>Control</i>	$Ts1(\lambda, \phi) = \begin{cases} 27 \left(1 - \sin^2\left(\frac{3\phi}{2}\right)\right)^\circ C & : -\frac{\pi}{3} < \phi < \frac{\pi}{3} \\ 0 & : \textit{otherwise} \end{cases}$
<i>FLAT</i>	$Ts2(\lambda, \phi) = \begin{cases} 27 \left(1 - \sin^4\left(\frac{3\phi}{2}\right)\right)^\circ C & : -\frac{\pi}{3} < \phi < \frac{\pi}{3} \\ 0 & : \textit{otherwise} \end{cases}$
<i>Q_{obs}</i>	$Ts3(\lambda, \phi) = (Ts1 + Ts2)/2$